



Title	Seed-dependent deposition behavior of A $\beta$ peptides studied with wireless quartz-crystal-microbalance biosensor
Author(s)	Ogi, Hirotsugu; Fukunishi, Yuji; Yanagida, Taiji et al.
Citation	Analytical Chemistry. 2011, 83(12), p. 4982-4988
Version Type	AM
URL	<a href="https://hdl.handle.net/11094/84185">https://hdl.handle.net/11094/84185</a>
rights	This document is the Accepted Manuscript version of a Published Work that appeared in final form in Analytical Chemistry, © American Chemical Society after peer review and technical editing by the publisher. To access the final edited and published work see <a href="https://doi.org/10.1021/ac2007703">https://doi.org/10.1021/ac2007703</a> .
Note	

*The University of Osaka Institutional Knowledge Archive : OUKA*

<https://ir.library.osaka-u.ac.jp/>

The University of Osaka

**Seed-dependent deposition behavior of A $\beta$  peptides studied with wireless quartz-crystal-microbalance biosensor**

Journal:	<i>Analytical Chemistry</i>
Manuscript ID:	ac-2011-007703.R1
Manuscript Type:	Article
Date Submitted by the Author:	n/a
Complete List of Authors:	Ogi, Hirotsugu; Osaka University, Graduate School of Engineering Science Fukunishi, Yuji; Osaka University Yanagida, Taiji; Osaka University Yagi, Hisashi; Osaka University, Institute for Protein Research Goto, Yuji; Osaka University, Institute for Protein Research Fukushima, Masahiko; Osaka University Uesugi, Kentaro; Osaka University Hirao, Masahiko; Osaka University

SCHOLARONE™  
Manuscripts

# Seed-dependent deposition behavior of A $\beta$ peptides studied with wireless quartz-crystal-microbalance biosensor

Hirotsugu Ogi,<sup>\*,†</sup> Yuji Fukunishi,<sup>†</sup> Taiji Yanagida,<sup>†</sup> Hisashi Yagi,<sup>‡</sup> Yuji Goto,<sup>‡</sup>  
Masahiko Fukushima,<sup>†</sup> Kentaro Uesugi,<sup>†</sup> and Masahiko Hirao<sup>†</sup>

*Graduate School of Engineering Science, Osaka University, Machikaneyama 1-3, Toyonaka, Osaka 560-8531, Japan, and Institute for Protein Research, Osaka University, Yamadaoka 3-2, Suita, Osaka 565-0871, Japan*

E-mail: ogi@me.es.osaka-u.ac.jp

## Abstract

Real-time monitoring of deposition processes of A $\beta$ 1-40 and A $\beta$ 1-42 peptides on various seeds has been performed using 55-MHz wireless quartz-crystal microbalance (QCM) over long-time periods ( $\sim$ 40 h). Dissolved peptide solutions were stirred for nucleation and growth of seeds at pH=7.4 and 4.6, which were immobilized on the sensor chips. The isolated A $\beta$  peptides were then flowed at the neutral pH, focusing on the interaction between the seeds and the monomers (or small multimers), excluding other interactions among seeds and other aggregates. The thioflavin-T fluorescence assay and atomic-force microscopy were used for evaluating structures of the seeds and deposited aggregates. The deposition rate, determined by the frequency decrease, is about 100 monomers/nm<sup>2</sup>/year, in the case of fibril formation.

---

\*To whom correspondence should be addressed

<sup>†</sup>Graduate School of Engineering Science

<sup>‡</sup>Institute for Protein Research, Osaka University, Yamadaoka 3-2, Suita, Osaka 565-0871, Japan

1  
2  
3 The notable deposition behavior was observed in the deposition of A $\beta$ 1-40 peptide on A $\beta$ 1-42  
4 seeds grown at the lower pH, which can be an important model for Alzheimer's disease.  
5  
6  
7  
8

## 9 10 **Introduction**

11  
12 Aggregation process of amyloid fibrils have received intensive studies in the last decade, because it  
13 is deeply involved in pathogenic mechanisms of Alzheimer's disease (AD).<sup>1-3</sup> Principal targets are  
14 the full-length peptides, A $\beta$ 1-40 (A $\beta$ 40) and A $\beta$ 1-42 (A $\beta$ 42), which cause proteinaceous deposits  
15 in central nervous systems.<sup>4,5</sup> They are extracted from the parental amyloid precursor proteins  
16 by enzymes or enzyme complexes,<sup>6</sup> and their concentrations are normally controlled by specific  
17 enzymes and antibodies in the cortical area of the brain.<sup>5</sup> A $\beta$ 40 is predominantly produced, but  
18 A $\beta$ 42 is reported to be more hydrophobic to cause fibril formation<sup>7</sup> and more neurotoxic.<sup>8</sup> Thus,  
19 understanding of the aggregation mechanism of the full-length peptides remains a central issue in  
20 the peptide polymerization study.  
21  
22  
23  
24  
25  
26  
27  
28  
29  
30

31  
32 Most previous works studied their aggregation process in bulk solutions.<sup>7,9-12</sup> However, inter-  
33 actions among seeds, aggregates, and monomers dominate the polymerization process for oligomers  
34 and fibrils in this case, blinding the most important interaction between the nuclei and surrounding  
35 peptides. In-situ monitoring of a single-fibril growth has been recently made possible.<sup>13-18</sup> These  
36 studies provided essential properties in the kinetics of the fibril formation, including the critical  
37 concentration for the fibril growth and nonmonotonic growth behavior (stop-and-go growth).<sup>14,17,18</sup>  
38 However, these methods fail to estimate macroscopic aggregation rate, including aggregations for  
39 oligomers and other amorphous phases: It is important to quantitatively know the aggregation rate  
40 of the peptides on various seeds, including oligomeric-phase growth as well as the fibril growth,  
41 because of higher neurotoxicity of oligomers than fibrils.<sup>19,20</sup>  
42  
43  
44  
45  
46  
47  
48  
49  
50  
51

52  
53 Macroscopic and quantitative analysis of interactions between proteins has been made possible  
54 with high-frequency quartz-crystal microbalance (QCM) biosensors.<sup>21-26</sup> They use change in the  
55 resonance frequency of quartz plate for the mass detection, which is caused by the additional  
56  
57  
58  
59  
60

1  
2  
3 inertia effect by the adsorbed proteins on the quartz surfaces. Although the viscosity effect would  
4 participate into the frequency change, high-frequency oscillator can make this effect negligible.<sup>26</sup>  
5  
6

7  
8 In this study, we systematically investigate the deposition behaviors of A $\beta$ 40 and A $\beta$ 42 pep-  
9 tides on various seeds using the homebuilt wireless quartz-crystal microbalance (W-QCM) biosen-  
10 sor with fundamental resonance frequency about 55 MHz.<sup>27</sup> First, we investigate the binding re-  
11 action between A $\beta$ 42 peptide and anti-A $\beta$  antibody to confirm the hydrophobicity of immobilized  
12 peptides and to show the sensitivity of our W-QCM. Then, we monitor the deposition behaviors  
13 of the peptides at a neutral pH on different seeds. The nucleation and growth of the seed is per-  
14 formed by stirring the isolated peptide solution in two different-pH solutions (pH=7.4 and 4.6)  
15 with different stirring time (0-168 h). The  $\beta$ -sheet contribution is evaluated by the thioflavin T  
16 (ThT) fluorescence. Structures of the seeds and those of deposits are observed by atomic-force  
17 microscopy (AFM). The most important observation is that A $\beta$ 40 peptide shows significantly high  
18 deposition rate on the A $\beta$ 42 seeds grown at the low pH.  
19  
20  
21  
22  
23  
24  
25  
26  
27  
28  
29  
30  
31

## 32 **Experimental Section**

### 33 **Wireless QCM and flow-injection system**

34  
35  
36 We used the originally developed wireless QCM system, whose details appear in previous stud-  
37 ies.<sup>27</sup> 30- $\mu$ m-thick AT-cut blank quartz plates with 3 mm diameter were used. The surface modi-  
38 fied sensor crystals were set in the homebuilt flow-injection system.<sup>26</sup> A micropump ran the carrier  
39 solution of phosphate buffered saline (PBS; pH=7.4) solution with 100-mM NaCl at a flow rate of  
40 500  $\mu$ l/min. When the A $\beta$  peptide solution flowed, it returned to the injection vial after the flow  
41 in the QCM cell; the peptide solution was circulated for a long-time monitoring of the deposition  
42 reaction. The temperature of the QCM cell was maintained at 37 $\pm$ 0.05 $^{\circ}$ C. The minimum mean-  
43 ingful frequency shift is about 2 Hz, and the Q factor of the system is between 1000 and 2500  
44 in the solution flow, depending on the gripping condition of the sensor chip. (Note that very thin  
45 quartz resonators were manually set in the sensor cell.)  
46  
47  
48  
49  
50  
51  
52  
53  
54  
55  
56  
57  
58  
59  
60

## Preparation of seeds and flowing solution

The lyophilized A $\beta$  peptides were dissolved in dimethyl sulfoxide (DMSO), and diluted to a final concentration of 12 $\mu$ M either by the PBS solution or by an acetic acid-sodium acetate buffer solution (ABS) to prepare two different pH values of 7.4 or 4.6, respectively. The prepared solutions were stirred to form the seeds, whose configurations were varied by the stirring time. We used ThT fluorescence to evaluate the degree of the  $\beta$ -sheet structure in the seeds.

The flowing solutions were prepared by the same procedure shown above, using the PBS buffer with 100 mM NaCl (pH=7.4). Thus, depositions proceed at the neutral pH.

## Immobilization of seeds on sensor chips

We deposited 1-nm Cr thin film and then 9-nm Au film on both surfaces of the quartz plates to immobilize the seeds via the gold-alkanethiol binding reaction. The AFM observation confirmed a flat Au surface with a roughness of  $R_a=0.4$  nm. The quartz crystals were cleaned in a piranha solution (98% H<sub>2</sub>SO<sub>4</sub>:33% H<sub>2</sub>O<sub>2</sub>=4:1) for 10 min, and after rinsing with ultrapure water several times, they were immersed in a 10  $\mu$ M 10-carboxy-1-decanethiol/ethanol solution for 24 h. The sensor surfaces were then activated using a 100 mM 1-ethyl-3-(3-dimethylaminopropyl)carbodiimide, hydrochloride (EDC) solution for 1 h at 37 °C. The crystals were then immersed in the seed solution for 24 h at 4 °C, and after the rinsing procedure with the PBS, they were immersed in a 10 mM aminoethyl-polyethylene glycol(NH<sub>2</sub>-PEG)/PBS solution to block the remaining activated sites to avoid nonspecific binding with flowing peptides. The sensor crystals were then set in the handmade sensor cell.

## Thioflavin T fluorescence measurement

The benzothiol-dye ThT specifically binds to  $\beta$ -sheets constructing amyloid fibrils and produces enhanced light emission.<sup>28,29</sup> The ThT fluorescence assay has been then used for evaluating formation of protofibrils and their extension.<sup>14–16,30</sup> We measured the ThT fluorescence level in the

1  
2  
3  
4 seed solutions and in the flowing solutions: The stock solution for the ThT assay was prepared by  
5 dissolving ThT in a glycine/sodium-hydroxide buffer solution (pH=8.5) with a final concentration  
6 of 5  $\mu$ M. A 100- $\mu$ l sample solution was mixed with 1-ml stock solution, and the mixture solution  
7 was poured into a quartz-glass cell for the fluorospectrophotometer. The ThT fluorescence level  
8 was measured as the fluorescence at 490 nm with the excitation at 450 nm.  
9  
10  
11  
12  
13

## 14 15 **AFM measurement**

16  
17 The AFM observation was performed to evaluate the morphology on sensor chips before and after  
18 the deposition reaction. The tapping-mode measurement was adopted with a silicon cantilever with  
19 the stiffness of 40 N/m, showing the resonance frequency near 300 kHz. The scan frequency was  
20 0.5 Hz.  
21  
22  
23  
24  
25  
26  
27

## 28 29 **Materials and Instruments**

30  
31 The lyophilized A $\beta$  peptides were obtained from Peptide Institute (4307-v for A $\beta$ 40 and 4349-v  
32 for A $\beta$ 42). The monoclonal anti-human A $\beta$  antibody was from Sigma (A 1349). The NH<sub>2</sub>-PEG  
33 (molecular weight: 3,000) was from Fluka (No. 07969). The 10-carboxy-1-decanethiol and EDC  
34 were from Dojindo (C385 and W001, respectively). PBS, ABS, DMSO, ThT were from Wako Pure  
35 Chemical Industries, Ltd. The AFM system was produced by Shimadzu Co. Ltd. (SPMAJ9600).  
36 ThT fluorescence was measured by a fluorescence spectrometer by JASCO Corporation (FP-6200).  
37  
38  
39  
40  
41  
42  
43  
44  
45

## 46 47 **Results**

### 48 49 **Monitoring of binding reaction between A $\beta$ 42 and anti-A $\beta$ antibody**

50  
51 Figure 1 shows the change in the amount of frequency decrease during binding reaction for various  
52 concentrations of the antibody solutions injected.  
53  
54  
55  
56  
57  
58  
59  
60

## Deposition on homogeneous peptide seeds

Figure 2 shows frequency evolutions during the deposition reactions of the peptides on their homogeneous seeds grown at pH=7.4. (The time for the seed nucleation is shown inside the frames.) In this study, we evaluate the deposition rate from the amount of the deposited monomer by 40 h in unit area in unit time, which was calculated by the Sauerbrey equation<sup>31</sup> and the effective area of the sensor chip, assuming purely mass loading effect on the frequency shift. This result is shown in Figs. 3(a) and (b) for homogenous depositions. (For example, the deposition rate of 100 monomers/nm<sup>2</sup>/year corresponds that 100 A $\beta$  peptides are deposited in the area of 1 nm<sup>2</sup> every year.) The deposition behavior of A $\beta$ 40 peptide is nearly independent of the seed structure, while that of A $\beta$ 42 peptide is significantly dependent on the time for seed nucleation.

The AFM micrographs on the sensor chips before and after the deposition reactions are shown in Figs. 4 and 5. We observe similar structures among seeds of A $\beta$ 40 grown for different stirring times; we fail to observe any fibril structures on the sensor chip but find spherical aggregates (Figs. 4 (a)-(c)). Also, we principally observe fibril structures after the deposition reaction for 40 h, being independent of the time for seed nucleation (Figs. 4(d)-(f)).

On the other hand, we see significant difference in the seed structure in the case of A $\beta$ 42. As the time for seed nucleation increases, the diameter of the spherical aggregate increases (Figs. 5(a)-(c)). However, a longer nucleation time ( $\sim$ 90 h or longer) caused smaller acute seeds ( $\sim$ 50 nm) and their beaded seeds (Fig. 5(d)). The deposited structures are dependent on the seeds: The spherical seeds yielded oligomeric deposits involving no fibrils (Figs. 5(e)-(g)), whereas the acute and beaded seeds caused well grown fibril structures (Fig. 5(h)).

## Deposition on heterogeneous peptide seeds

Figures 3(c) and (d) show the deposition rates of the peptides on the seeds grown at pH=7.4 and 4.6, respectively. Notable observation is that A $\beta$ 40 peptide shows a high deposition rate on the A $\beta$ 42 seeds nucleated at the lower pH (40/42 in Fig. 3(d)), and that the deposited structure shows oligomeric conformation without fibrils (Fig. 6 (b)), unlike the other cases of the A $\beta$ 40-peptide

1  
2  
3 deposition. This high deposition behavior is also confirmed by our multichannel QCM,<sup>27</sup> where  
4 we can monitor the deposition behaviors on different sensor chips simultaneously with the same  
5 flowing solution. Figure 7 shows the result, confirming the high deposition rate of A $\beta$ 40 on A $\beta$ 42  
6 seeds grown at the lower pH. The A $\beta$ 42 seeds grown at pH=4.6 (Fig. 6(a)) are non-spherical  
7 aggregates and their diameter ( $\sim$ 50 nm) is smaller than those grown at pH=7.4 (Fig. 5 (c)).  
8  
9  
10  
11  
12  
13

## 14 15 **ThT fluorescence measurement**

16  
17  
18 Figure 8 shows the change in the ThT fluorescence intensity caused by the stirring procedure for  
19 nucleation of seeds. The ThT fluorescence level appears to increase with the increase in the stirring  
20 time, indicating formation of  $\beta$ -sheet structures in the seeds, except for the A $\beta$ 42 seed grown at  
21 pH=4.6: The ThT fluorescence in this case remains lower, close to the baseline. We also monitored  
22 the change in the ThT fluorescence levels in the flowing solutions, which were nearly the baseline  
23 value.  
24  
25  
26  
27  
28  
29  
30  
31  
32

## 33 **Discussion**

### 34 **Recognition of hydrophobic amino acids by antibody**

35  
36  
37 We immobilized the peptide seeds on the sensor surfaces covalently using the self-assembled  
38 monolayer via their amino terminals. Such a tight binding may affect the hydrophobic nature  
39 of the peptide. Because major hydrophobic amino acids are located from middle part to the car-  
40 boxyl end, the hydrophobicity of the immobilized peptide can be confirmed using an antibody,  
41 which recognizes the middle-part hydrophobic amino acids as the epitope. We then used the mon-  
42 oclonal anti-A $\beta$  antibody, which recognizes the middle part hydrophobic amino acids between 17  
43 and 24. Figure 1 exhibits significant frequency change by the injection of the monoclonal anti-  
44 body. Because the antibody recognizes the middle-part amino acids, the hydrophobic nature of  
45 amino acids from middle to the carboxyl end remains active, which is important for the peptide  
46  
47  
48  
49  
50  
51  
52  
53  
54  
55  
56  
57  
58  
59  
60

1  
2  
3 deposition. Thus, we expect that the deposition behavior on immobilized peptides and seeds will  
4 proceed without being affected by the covalent immobilization treatment.  
5  
6

7 We evaluate the affinity between the immobilized peptide and the monoclonal antibody: In a  
8 flow-injection system, the frequency change obeys the exponential law with the exponential coef-  
9 ficient  $\alpha = C_A k_a + k_d$ , where  $k_a$  and  $k_d$  denote the association and dissociation velocity constants,  
10 respectively, and  $C_A$  is the concentration of the analyte injected.<sup>32,33</sup> Thus, the equilibrium con-  
11 stant  $K_A$  is given by  $K_A = k_a/k_d$ . By fitting the exponential function to the observed frequency  
12 change, we obtained the exponential constant with various analyte concentrations, and determined  
13  $k_a$  and  $k_d$ , and then  $K_A$  value from their relationship as  $K_A = 3.5 \times 10^7 \text{ M}^{-1}$ . This value is acceptable  
14 as a binding affinity between antigen-antibody reactions and is significantly higher than that of  
15 nonspecific binding ( $K_A < \sim 10^5 \text{ M}^{-1}$ ),<sup>34</sup> confirming that the antigen-antibody reaction was moni-  
16 tored. The result in Fig. 1 shows the successful detection of a low concentration analyte ( $\sim 7 \text{ pM}$ ),  
17 demonstrating the high sensitivity of the W-QCM. This supports the high capability of monitoring  
18 the A $\beta$  peptide deposition, whose molecular mass ( $\sim 4500 \text{ Da}$ ) is relatively smaller and difficult to  
19 be detected with a conventional low-frequency QCM.  
20  
21  
22  
23  
24  
25  
26  
27  
28  
29  
30  
31  
32  
33  
34  
35

### 36 Homogenous deposition

37  
38 First, we discuss importance of our success in the long-time monitoring over 40 h of the deposition  
39 reaction of A $\beta$  peptides on immobilized nuclei, which has never been achieved previously with a  
40 QCM. In the past, in-situ AFM studies provided essential aggregation behavior of peptides in early  
41 stages.<sup>13,17</sup> However, because of the short time monitoring ( $< \sim 2 \text{ h}$ ) focusing only on a measurable  
42 target, the global aggregation rate cannot be determined. The direct monitoring on a single fibril by  
43 a total reflection microscopy with the fluorescence assay<sup>14-16</sup> revealed very important characteris-  
44 tics of the fibril growth, including the stop-and-go growth. This approach is, however, unavailable  
45 to monitoring of aggregation behavior of non- $\beta$  sheet structures because of insensitivity of the low  
46 affinity of ThT to non- $\beta$  structures. Thus, macroscopic and quantitative deposition monitoring for  
47 a long time has been required to systematically investigate the deposition behavior of peptides on  
48  
49  
50  
51  
52  
53  
54  
55  
56  
57  
58  
59  
60

1  
2  
3 seeds without involving interactions between seeds. The deposited structures on seeds are actu-  
4 ally different from those formed solely by stirring the solution. For example, in Fig. 4(c), we  
5 observe spherical aggregates of A $\beta$ 40 in the seed solution stirred for 168 h, but the deposits onto  
6 6-h and 48-h seeds predominantly consist of fibrils by 40 h. (Total incubation times are 46 and 88  
7 h, respectively, shorter than 168 h.) Therefore, the aggregated structure in the bulk solution will  
8 be governed by interactions among aggregates and ever-nucleating seeds, and not by interacting  
9 between specific seeds and monomers.  
10  
11

12  
13  
14  
15  
16  
17  
18 The seed-nucleation process for A $\beta$ 40 causes spherical aggregates with diameters of 30-100  
19 nm, and their forms are apparently independent of the nucleation time (Figs. 4(a)-(c)), except for  
20 the zero-seeding-time case (in this case, unnoticeable structure was observed with AFM because of  
21 smaller peptides immobilized). Because the ThT fluorescence increases (Fig. 8), the A $\beta$ 40 seeds  
22 should involve the  $\beta$ -sheet structures, potentializing the fibril nuclei. The resultant deposits by the  
23 peptide-solution flow principally consist of fibrils (Figs. 4(d)-(f)). Pathway for fibril formation  
24 from monomer peptides is complicated in bulky solutions and experiences multistep aggregates,  
25 including oligomers,<sup>35,36</sup> non- $\beta$  seeds,<sup>12</sup> and protofibrils.<sup>10,11,13</sup> Thus, it has never been straight-  
26 forward to evaluate the aggregation rate with previous methods because different mechanisms for  
27 the fibril formation could be involved. In contrast, the deposition monitoring with our QCM can  
28 narrowly focus on the mechanism of the single-peptide deposition on the nuclei, excluding other  
29 interactions. The initial dissolving preparation of the peptide would, however, involve smaller ag-  
30 gregates of multimers as well as monomers.<sup>11</sup> We therefore centrifuged the dissolved solutions  
31 before the injection using a 10-kDa filtration tube for 30 min with 8000g to remove the initial  
32 aggregates (if any), which yielded identical results to those in Fig. 2. Thus, the peptide dissolving  
33 solutions mainly contain monomers and dimers. The ThT fluorescence level also remained the  
34 baseline value in the flowing solution (broken line in Fig. 8), indicating insignificant growth of  
35 seeds in the flowing solution. Observations in Fig. 3(a) and Figs. 4(d)-(f) show that both the de-  
36 position rate and deposited structures are nearly independent of the seed, including the deposition  
37 on immobilized monomers (0 h seed-nucleation time). In this case, the hydrophobic amino acids  
38  
39  
40  
41  
42  
43  
44  
45  
46  
47  
48  
49  
50  
51  
52  
53  
54  
55  
56  
57  
58  
59  
60

1  
2  
3  
4  
5  
6  
7  
8  
9  
10  
11  
12  
13  
14  
15  
16  
17  
18  
19  
20  
21  
22  
23  
24  
25  
26  
27  
28  
29  
30  
31  
32  
33  
34  
35  
36  
37  
38  
39  
40  
41  
42  
43  
44  
45  
46  
47  
48  
49  
50  
51  
52  
53  
54  
55  
56  
57  
58  
59  
60

faced outward can be the seed source eventually for fibrils. We expect that protofibrils are involved in the A $\beta$ 40 seeds, and the peptides accumulate to grow the fibrils structures. Thus, nearly constant deposition rate of  $\sim 100$  monomers/nm<sup>2</sup>/year (Fig. 3(a)) is expected to represent the rate of an A $\beta$ 40 peptide to be adsorbed on the nuclei to grow the fibril.

In the case of the A $\beta$ 42 peptide, paranuclei and oligomeric aggregates are immediately formed after the peptide dissolution.<sup>11</sup> In our observation, the diameter of the spherical seed increases (Figs. 5(a)-(c)) and the deposition rate raises (Fig. 3(b)) as the time for seed nucleation increases. The oligomeric aggregates enlarge by adsorbing monomers, multimers, and paranuclei in the flowing solution (Figs. 5(e)-(g)), and the number of the adsorption site on their surfaces will be increased as their growth, resulting in the increase in the deposition rate. Because the ThT fluorescence increases as the seed-nucleation time at pH=7.4 (Fig. 8), the immobilized seeds are expected to involve  $\beta$ -sheet structures. However, the resultant deposited structures are apparently oligomeric aggregates, and we cannot see any fibrils when the seed-nucleation time is shorter than  $\sim 60$  h. On the other hand, when the seed-nucleation time is long enough, fibril structures are clearly observed after the deposition reaction (Fig. 5(h)), and the deposition rate becomes as high as that in the deposition of A $\beta$ 40 for fibrils. In this case, the immobilized seeds consist of smaller ( $\sim 50$  nm) and acute aggregates and their beaded structures, which are similar with structures reported previously.<sup>10,11</sup> We consider that they are protofibrils or related structures and significantly adsorb monomers and multimers in the flowing solution for the growth of the fibril structures (Fig. 5(h)). Therefore, a long-time incubation procedure is needed to engender protofibrillar structures, which is in agreement with previous reports.<sup>10,13</sup> It is important to note the close deposition rates in achieving fibril structures ( $\sim 100$  monomers/nm<sup>2</sup>/year) both for A $\beta$ 40 and A $\beta$ 42 peptides (Figs. 3(a) and 90 h in (b)), indicating that the kinetics of the peptide deposition purely for fibril growth is similar between the two peptides.

## Heterogeneous deposition

The most important observation in this study is the result in Fig. 3(d) and Fig. 7, where A $\beta$ 40 peptides significantly accumulate on the A $\beta$ 42 seeds grown at pH=4.6, resulting in oligomeric deposits (Fig. 6(b)). This deposition rate is much higher than those in other cases for seeds grown at the lower pH and is comparable with those of the homogeneous depositions for the fibril formation ( $\sim 100$  monomers/nm<sup>2</sup>/year). The seed structure in this case (Fig. 6(a)) is significantly different from that grown at pH=7.4 (Fig. 5(c)), consisting of smaller non-spherical aggregates. The ThT fluorescence keeps low level, close to the baseline, during the nucleation of the A $\beta$ 42 seed at pH=4.6 (Fig. 8). Previous work shows that non- $\beta$  structures formed during incubation can transform into  $\beta$ -sheet fibril structures.<sup>12</sup> However, we cannot see such a transformation in our result: The non- $\beta$  seeds of A $\beta$ 42 grow oligomeric structures by adsorbing A $\beta$ 40 peptides and fail to form any fibrils despite the long deposition time ( $\sim 40$  h).

The deposition of A $\beta$ 40 peptides on A $\beta$ 42 seeds grown at pH=7.4 also caused oligomeric structures (40/42 in Fig. 3(c)). In this case, the seeds should involve  $\beta$  structures because of their higher ThT fluorescence level, but the deposition rate is smaller than that on the seeds grown at pH=4.6. Jarrett et al.<sup>7</sup> indicated that small amounts of A $\beta$ 42 seeds could enhance fibril formation in A $\beta$ 40 peptides, which disagrees with our result for the A $\beta$ 42 seeds grown at pH=7.4, yielding the smaller deposition rate. We attribute this discrepancy to the bulk solution used in the previous study, where interactions among aggregates of A $\beta$ 40 peptides, involving the A $\beta$ 42 core, would cause transformation of the non- $\beta$  structure aggregates into protofibrils  $\beta$  structures,<sup>12</sup> enhancing the fibril formation. Our method here monitors nearly pure interaction between monomers (and small multimers) and seeds, revealing that deposition of A $\beta$ 40 peptides onto A $\beta$ 42 seeds forms oligomeric structures without fibrils.

The deposition of A $\beta$ 42 peptide on A $\beta$ 40 seeds grown at pH=7.4 caused fibril structures, and its deposition rate is larger (42/40 in Fig. 3(c)). The ThT fluorescence level of the A $\beta$ 40 seed is higher, and we consider that the protofibrils in the A $\beta$ 40 seeds yielded the fibril structure even for the deposition of A $\beta$ 42 peptide, unlike the oligomeric structure on A $\beta$ 42 seeds with the same

1  
2  
3 nucleation time (42/42 in Fig. 3(c)).  
4

5 The deposition rates on seeds grown at pH=4.6 are significantly smaller than those in other  
6 cases. This will be explained by relatively lower ThT fluorescence level of the seeds. Wood et al.<sup>9</sup>  
7 reported that aggregation of A $\beta$ 40 peptide onto A $\beta$ 40 seeds grown at a low pH was decelerated,  
8 which agrees with our observation (40/40 in Fig. 3(d)). Thus, seeds formed at lower pH shows low  
9 activity for the peptide adsorption, except for the special case of the deposition of A $\beta$ 40 on A $\beta$ 42  
10 seeds as described above.  
11  
12  
13  
14  
15  
16

17 We consider that this special case can be an important model for AD. Oligomers and re-  
18 lated structures are more neurotoxic than fibrils,<sup>1,19,20,37</sup> and significant aggregation behavior of  
19 oligomeric structures are required for an AD model. A $\beta$ 42 is more hydrophobic and will be self-  
20 associate just after its production from the amyloid precursor protein by the cleaving enzymes ( $\beta$   
21 and  $\gamma$  secretases<sup>6</sup>), which show high activity at lower pH. Therefore, the isolated A $\beta$ 42 peptides  
22 can form the seeds immediately at lower pH environment, and they diffuse inside and outside cells  
23 for neutral pH environments, with which A $\beta$ 40 peptides interact more frequently, because most of  
24 the produced peptides is A $\beta$ 40 ( $\sim$ 90 %).<sup>38-40</sup> Thus, the large amount of A $\beta$ 40 peptides deposits  
25 on the A $\beta$ 42 seeds to cause and grow oligomeric structures.  
26  
27  
28  
29  
30  
31  
32  
33  
34  
35  
36  
37

## 38 Conclusion

39 We achieved following four principal conclusions in this study: (i) The wireless QCM success-  
40 fully monitors the long-time deposition behavior of A $\beta$  peptides on their nuclei over 40 h. (ii)  
41 A $\beta$ 40 peptide shows nearly constant deposition rate on A $\beta$ 40 seeds grown at the neutral pH. The  
42 deposition rate is about 100 monomers/nm<sup>2</sup>/year. The deposits show fibril structures. (iii) A $\beta$ 42  
43 peptides show significantly seed-dependent deposition behavior on A $\beta$ 42 seeds grown at the neu-  
44 tral pH. The deposition rate increases as the seed-nucleation time increases. It becomes higher for  
45 well-grown seed ( $\sim$ 100 monomers/nm<sup>2</sup>/year), yielding fibril structures, otherwise the deposition  
46 caused oligomeric structures. (iv) A $\beta$ 40 peptide shows notable deposition behavior on the A $\beta$ 42  
47  
48  
49  
50  
51  
52  
53  
54  
55  
56  
57  
58  
59  
60

1  
2  
3 seeds grown at a low pH(=4.6), resulting in oligomeric structures. The deposition rate is as high as  
4 those on seeds grown at the neutral pH for fibril structures and is much higher than other cases for  
5 depositions on seeds grown at the low pH.  
6  
7  
8  
9

## 10 11 **References**

- 12  
13  
14 (1) Lambert, M. P.; Barlow, A. K.; Chromy, B. A.; Edwards, C.; Freed, R.; Liosatos, M.; Morgan,  
15 T. E.; Rozovsky, I.; Trommer, B.; Viola, K. L.; Wals, P.; Zhang, C.; Finch, C. E.; Krafft, G. A.;  
16 Klein, W. L. *Proc. Natl. Acad. Sci. USA* 1998, 95, 6448-6453.  
17  
18  
19 (2) Bucciantini, M.; Giannoni, E.; Chiti, F.; Baroni, F.; Formigli, L.; Zurdo, J.; Taddei, N.; Ram-  
20 poni, G.; Dobson, C. M.; Stefani, M. *Nature* 2002, 416, 507-511.  
21  
22  
23 (3) Stefani, M.; Dobson, C. M. *J. Mol. Med.* 2003, 81, 678-699.  
24  
25  
26 (4) Younkin, S. G. *J. Physiol. Paris* 1998, 92, 289-292.  
27  
28  
29 (5) Iwata, N.; Tsubuki, S.; Takaki, Y.; Watanabe, K.; Sekiguchi, M.; Hosoki, E.; Kawashima-  
30 Morishima, M.; Lee, H. J.; Hama, E.; Sekine-Aizawa, Y.; Saido, T. C. *Nat. Med.* 2000, 6,  
31 143-150.  
32  
33  
34 (6) LaFerla, F. M.; Green, K. N.; Oddo, S. *Nat. Rev. Neurosci.* 8, 499-509.  
35  
36  
37 (7) Jarrett, J. T.; Berger, E. P.; Lansbury, Jr., P. T. *Biochem.* 1993, 32, 4693-4697.  
38  
39  
40 (8) Takahashi, R. H.; Milner, T. A.; Li, F.; Nam, E. E.; Edgar, M. A.; Yamaguchi, H.; Beal, M. F.;  
41 Xu, H.; Greengard, P.; Gouras, G. K. *Am. J. Pathol.* 2002, 161, 1869-1879.  
42  
43  
44 (9) Wood, S. J.; Maleeff, B.; Hart, T.; Wetzell, R. J. *Mol. Biol.* 1996, 256, 870-877.  
45  
46  
47 (10) Nybo, M.; Svehag, S.-E.; Nielsen, E. H. *Scand. J. Immunol.* 1999, 49, 219-223.  
48  
49  
50 (11) Bitan, G.; Kirkitadze, M. D.; Lomakin, A.; Vollers, S. S.; Benedek, G. B.; Teplow, D. B. *Proc.*  
51 *Natl. Acad. Sci. USA* 2003, 100, 330-335.  
52  
53  
54  
55  
56  
57  
58  
59  
60

- 1  
2  
3  
4 (12) Benseny-Cases, N.; Cocera, M.; Cladera, J. *Biochem. Biophys. Res. Commun.* 2007, 361,  
5 916-921.  
6  
7  
8  
9 (13) Blackley, H. K. L.; Sanders, G. H. W.; Davies, M. C.; Roberts, C. J.; Tendler, S. J. B.;  
10 Wilkinson, M. J. J. *Mol. Biol.* 2000, 298, 833-840.  
11  
12  
13 (14) Ban, T.; Hoshino, M.; Takahashi, S.; Hamada, D.; Hasegawa, K.; Naiki, H.; Goto, Y. *J. Mol.*  
14 *Biol.* 2004, 344, 757-767.  
15  
16  
17  
18 (15) Ban, T.; Morigaki, K.; Yagi, H.; Kawasaki, T.; Kobayashi, A.; Yuba, S.; Naiki, H.; Goto, Y.  
19 *J. Biol. Chem.* 2006, 281, 33677-33683  
20  
21  
22  
23 (16) Ban, T.; Yamaguchi, K.; Goto Y. *Acc. Chem. Res.* 2006, 39, 663-670.  
24  
25  
26 (17) Kellermayer, M. Z.; Karsai, Á.; Benke, M.; Soós, K.; Penke, B. *Proc. Natl. Acad. Sci. USA*  
27 2008, 105, 141-144.  
28  
29  
30  
31 (18) Ferkinghoff-Borg, J.; Fonslet, J.; Andersen, C. B.; Krishna, S.; Pigolotti, S.; Yagi, H.; Goto,  
32 Y.; Otzen, D.; Jensen, M. H. *Phys. Rev. E* 2010, 82, 010901(R).  
33  
34  
35  
36 (19) Klein, W. L.; Krafft, G. A.; Finch, C. E. *Trends Neurosci.* 2001, 24, 219-224.  
37  
38  
39 (20) Mastrangelo, I.A.; Ahmed, M.; Sato, T.; Liu, W.; Wang, C.; Hough, P.; Smith, S.O. *J. Mol.*  
40 *Biol.* 2006, 358, 106-119.  
41  
42  
43  
44 (21) Ogi, H.; Motohisa, K.; Matsumoto, T.; Hatanaka, K.; Hirao, M. *Anal. Chem.* 2006, 78, 6903-  
45 6909.  
46  
47  
48  
49 (22) Cooper, M. A.; Singleton, V. T. *J. Mol. Recognit.* 2007, 20, 154-184.  
50  
51  
52 (23) Natesan, M.; Cooper, M. A.; Tran, J. P.; Rivera, V. R.; Poli, M. A. *Anal. Chem.* 2009, 81,  
53 3896-3902.  
54  
55  
56 (24) Furusawa, H.; Ozeki, T.; Morita, M.; Okahata, Y. *Anal. Chem.* 2009, 81, 2268-2273.  
57  
58  
59  
60

- 1  
2  
3  
4 (25) Uttenthaler, E.; Schráml, M.; Mandel, J.; Drost, S. *Biosens. Bioelectron.* 2001, 16, 735-743.  
5  
6  
7 (26) Ogi, H.; Nagai, H.; Fukunishi, Y.; Hirao, M.; Nishiyama, M. *Anal. Chem.* 2009, 81, 8068-  
8 8073.  
9  
10  
11 (27) Ogi, H., Nagai, H.; Fukunishi, Y.; Yanagida, Y.; Hirao, M.; Nishiyama, M. *Anal. Chem.*  
12 2010, 82, 3957-3962.  
13  
14  
15  
16 (28) Naiki, H.; Higuchi, K.; Hosokawa, M.; Takeda, T. *Anal Biochem.* 1989, 177, 244-249.  
17  
18  
19 (29) Biancalana M.; Makabe K.; Koide A.; Koide S. *J. Mol. Biol.* 2009, 385, 1052-63.  
20  
21  
22 (30) Naiki, H.; Higuchi, K.; Matsushima, K.; Shimada, A.; Chen, W. H.; Hosokawa, M.; Takeda,  
23 T. *Lab Invest.* 1990, 62, 768-773.  
24  
25  
26  
27 (31) Sauerbrey, G. *Z. Phys.* 1959, 155, 206-222.  
28  
29  
30 (32) Ebara, Y.; Itakura, K.; Okahata, Y. *Langmuir.* 1996, 12, 5165-5170.  
31  
32  
33 (33) Liu, Y.; Yu, X.; Zhao, R.; Shangguan, D.; Bo, Z.; Liu, G. *Biosens. Bioelectron.* 2003, 19,  
34 9-19.  
35  
36  
37 (34) Ogi, H.; Fukunishi, Y.; Nagai, H.; Okamoto, K.; Hirao, M.; Nishiyama, M. *Biosens. Bioelec-*  
38 *tron.* 2009, 24, 3148-3152.  
39  
40  
41  
42 (35) Lomakin, A.; Chung, D. S.; Benedek, G. B.; Kirschner, D. A.; Teplow, D. B. *Proc. Natl.*  
43 *Acad. Sci. USA* 1996, 93, 1125-1129.  
44  
45  
46  
47 (36) Lomakin, A.; Teplow, D. B.; Kirschner, D. A.; Benedek, G. B. *Proc. Natl. Acad. Sci. USA*  
48 1997, 94, 7942-7947.  
49  
50  
51  
52 (37) Walsh, D. M.; Klyubin, I.; Fadeeva, J. V.; Cullen, W. K.; Anwyl, R.; Wolfe, M. S.; Rowan,  
53 M. J.; Selkoe, D. J. *Nature* 416, 535-539.  
54  
55  
56  
57  
58  
59  
60

- 1  
2  
3  
4 (38) Suzuki, N.; Cheung, T. T.; Cai, X.-D.; Odaka, A.; Otvos, L. Jr.; Eckman, C.; Golde, T. E.;  
5  
6     Younkin, S. G. 1994, *Science* 264, 1336-1340.  
7  
8  
9 (39) Iwatsubo, T.; Odaka, A.; Suzuki, N.; Mizusawa, H.; Nukina, N.; Ihara, Y. 1994, *Neuron* 13,  
10  
11     45-53.  
12  
13 (40) Gravina, S. A.; Ho, L. B.; Eckman, C. B.; Long, K. E.; Otvos, L., Jr.; Younkin, L. H.; Suzuki,  
14  
15     N.; Younkin, S. G. 1995, *J. Biol. Chem.* 270, 7013-7016.  
16  
17  
18  
19  
20  
21  
22  
23  
24  
25  
26  
27  
28  
29  
30  
31  
32  
33  
34  
35  
36  
37  
38  
39  
40  
41  
42  
43  
44  
45  
46  
47  
48  
49  
50  
51  
52  
53  
54  
55  
56  
57  
58  
59  
60

## Figure Caption

**Fig. 1** Binding curves between immobilized A $\beta$ 42 peptides and the monoclonal anti-A $\beta$  antibody to recognize the middle-part hydrophobic amino acids. The concentration of the antibody is varied between 6.7 pM and 67 nM.

**Fig. 2** (Color) Real-time monitoring of deposition behaviors of (a)A $\beta$ 40 and (b)A $\beta$ 42 peptides on their homogenous seeds. The frequency change  $\Delta f$  is proportional to the deposited mass on the sensor chips. The peptide concentrations are 12  $\mu$ M for both cases. The times for nucleation of seeds are shown.

**Fig. 3** The deposition rates (monomers/nm<sup>2</sup>/year) for depositions of (a)A $\beta$ 40 on A $\beta$ 40 seeds, (b)A $\beta$ 42 on A $\beta$ 42 seeds, (c)A $\beta$ 40 and A $\beta$ 42 on seeds grown at pH=7.4, and (d)A $\beta$ 40 and A $\beta$ 42 on seeds grown at pH=4.6. Symbols [F] and [O] mean that deposited structures are principally fibrils and oligomeric structures, respectively. The notation 40/42, for example, denotes the deposition of A $\beta$ 40 peptide on A $\beta$ 42 seed.

**Fig. 4** (Color) AFM images ( $2\mu\text{m}\times 2\mu\text{m}$ ) for A $\beta$ 40 seeds grown at pH=7.4 for (a)6 h, (b)48 h, and (c)168 h and for resultant structures by deposition of A $\beta$ 40 peptide for 40 h ((d), (e), and (f), respectively).

**Fig. 5** (Color) AFM images ( $2\mu\text{m}\times 2\mu\text{m}$ ) for A $\beta$ 42 seeds grown at pH=7.4 for (a)6 h, (b)24 h, (c)48 h, and (d)90 h and for resultant structures by deposition of A $\beta$ 42 peptide for 40 h ((e), (f), (g), and (h) respectively).

1  
2  
3  
4 **Fig. 6** (Color) AFM images ( $2\mu\text{m}\times 2\mu\text{m}$ ) for (a)  $A\beta_{42}$  seed grown at  $\text{pH}=4.6$  for 40 h and (b) resultant  
5 structure by deposition of  $A\beta_{40}$  peptide at  $\text{pH}=7.4$  for 40 h.  
6  
7  
8  
9

10 **Fig. 7** Deposition behaviors of  $A\beta_{40}$  peptides on  $A\beta_{42}$  seeds grown at  $\text{pH}=7.4$  and 4.6 monitored  
11 by the multichannel wireless QCM simultaneously.  
12  
13  
14  
15  
16

17 **Fig. 8** Evolutions of ThT fluorescence intensity by stirring the peptide solution. In the flowing  
18 solution, the ThT fluorescence remained the baseline level.  
19  
20  
21  
22  
23  
24  
25  
26  
27  
28  
29  
30  
31  
32  
33  
34  
35  
36  
37  
38  
39  
40  
41  
42  
43  
44  
45  
46  
47  
48  
49  
50  
51  
52  
53  
54  
55  
56  
57  
58  
59  
60

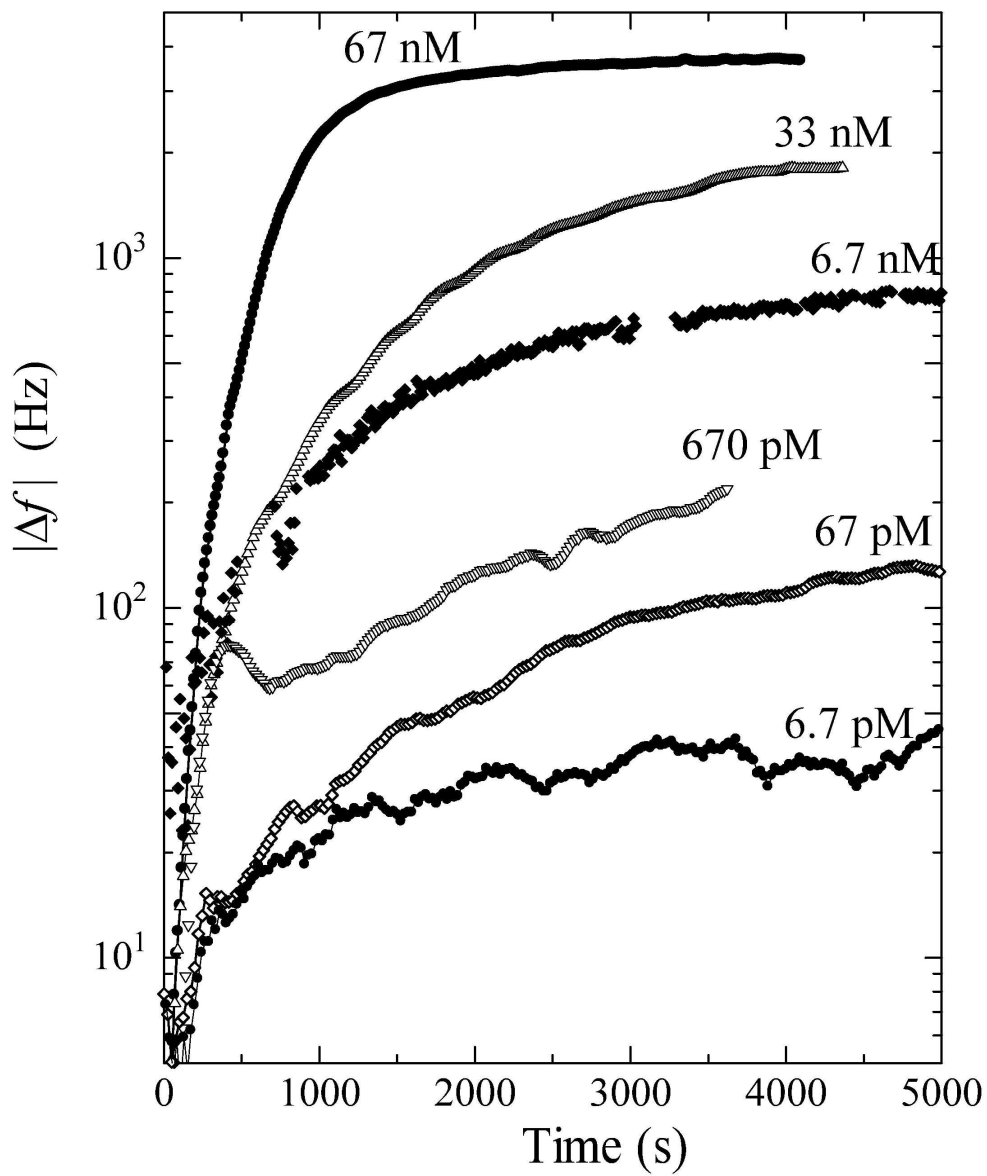


Fig. 1  
188x224mm (600 x 600 DPI)

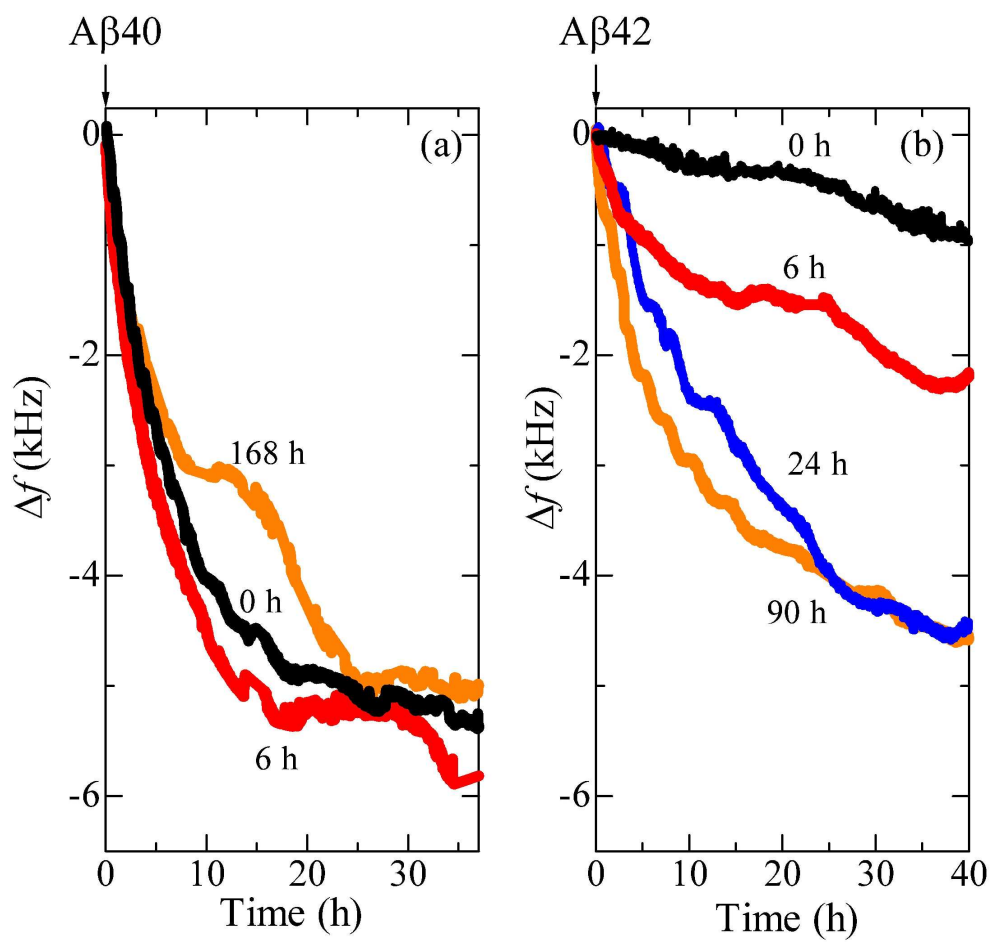


Fig. 2  
188x179mm (600 x 600 DPI)

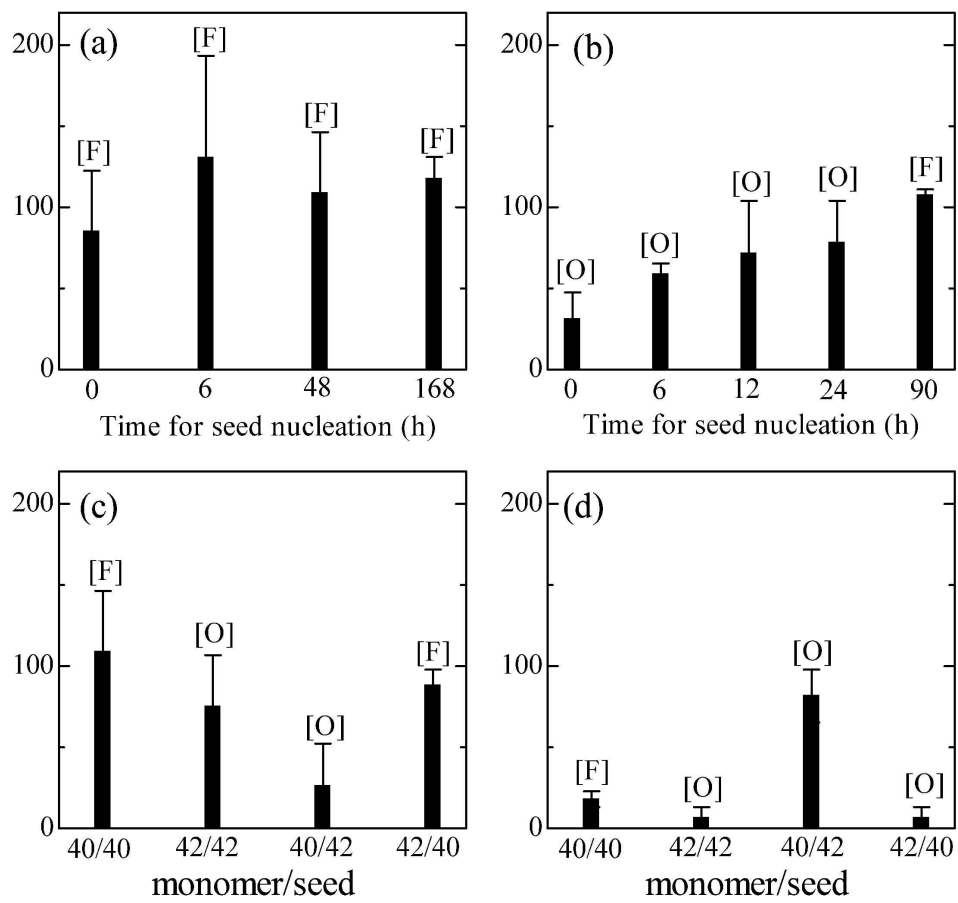


Fig. 3  
196x181mm (600 x 600 DPI)

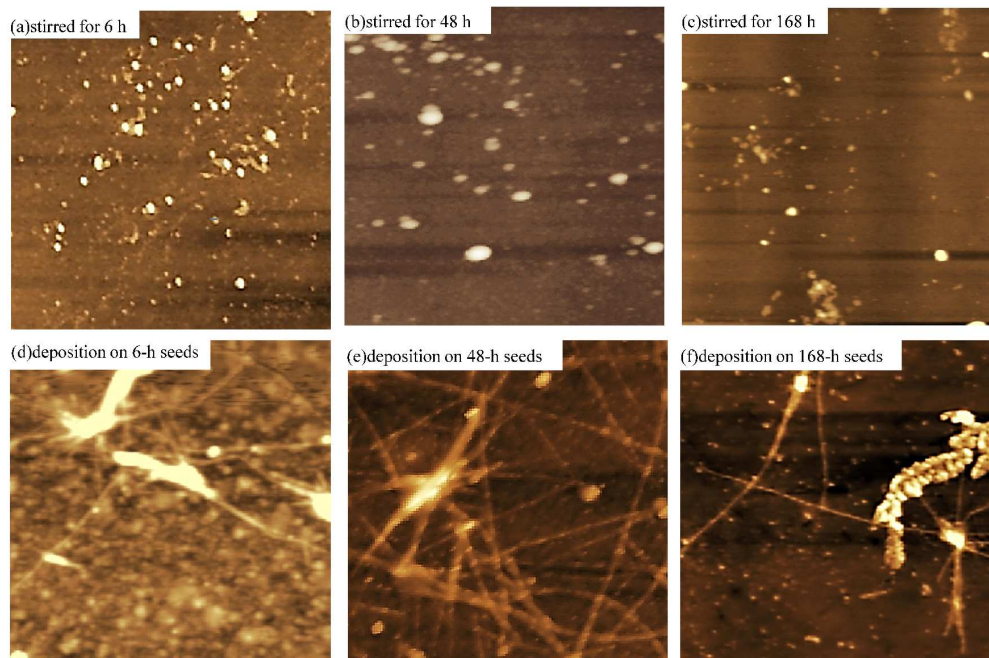


Fig. 4  
298x196mm (600 x 600 DPI)

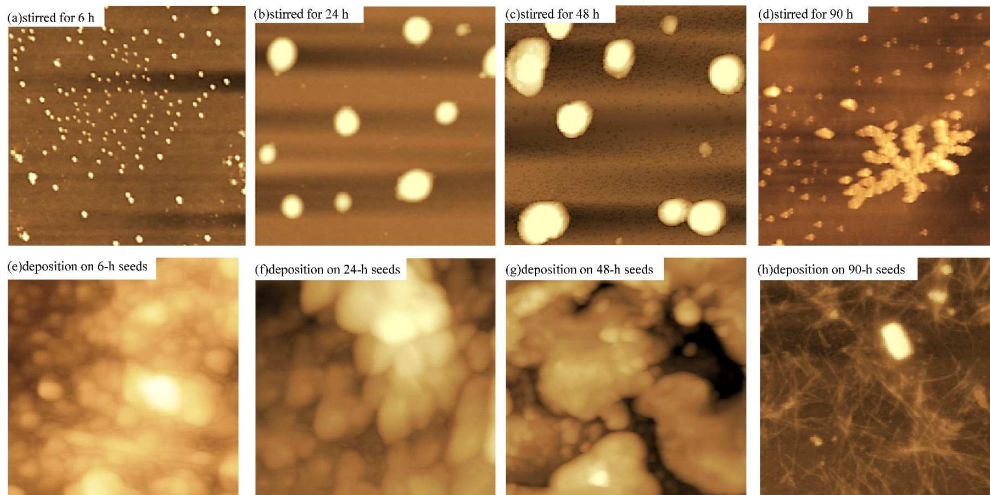


Fig. 5  
386x192mm (600 x 600 DPI)

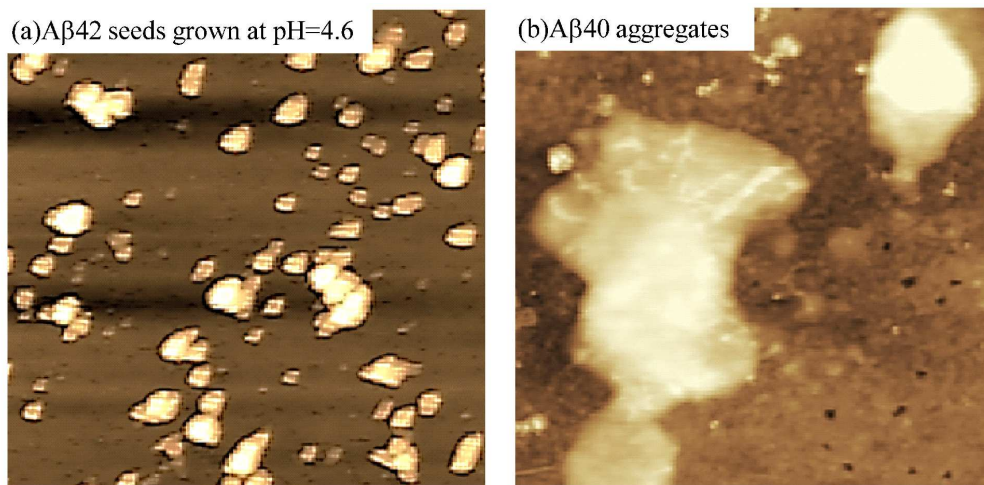


Fig. 6  
245x119mm (600 x 600 DPI)

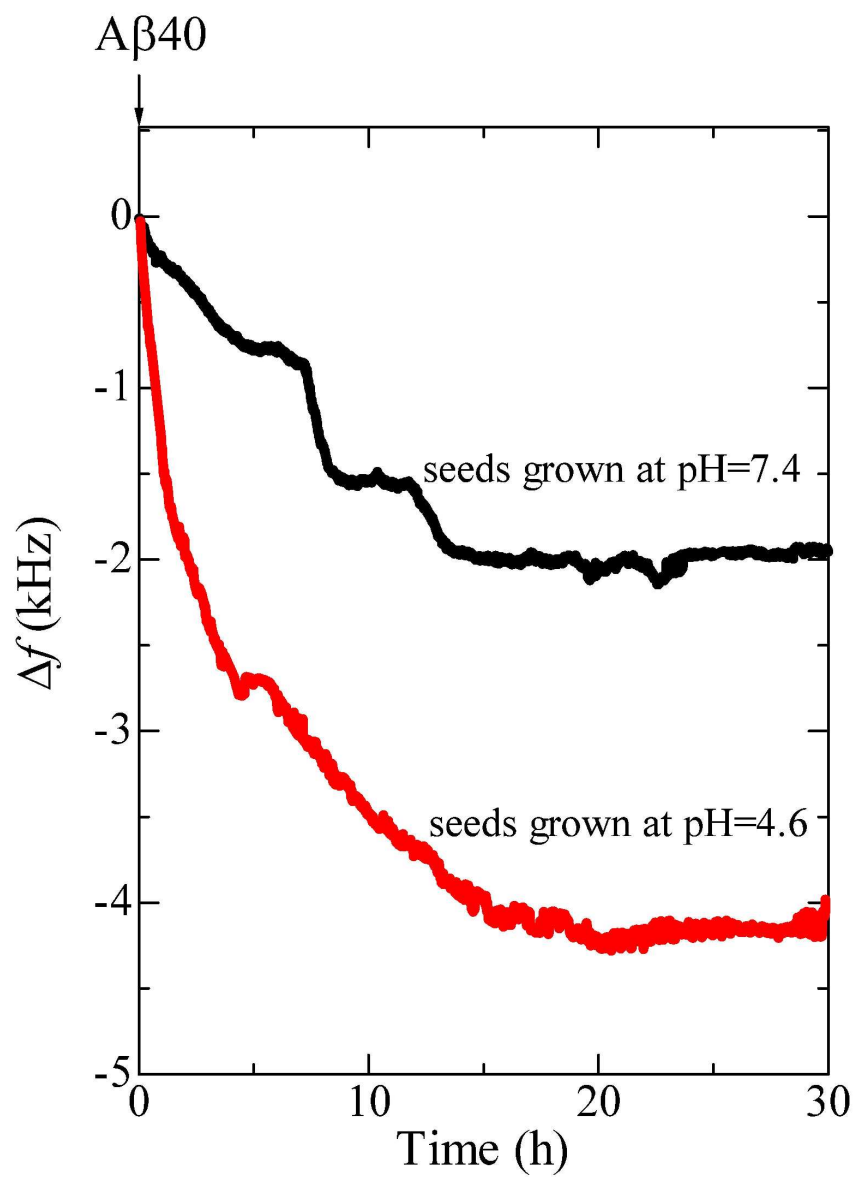


Fig. 7  
137x186mm (600 x 600 DPI)

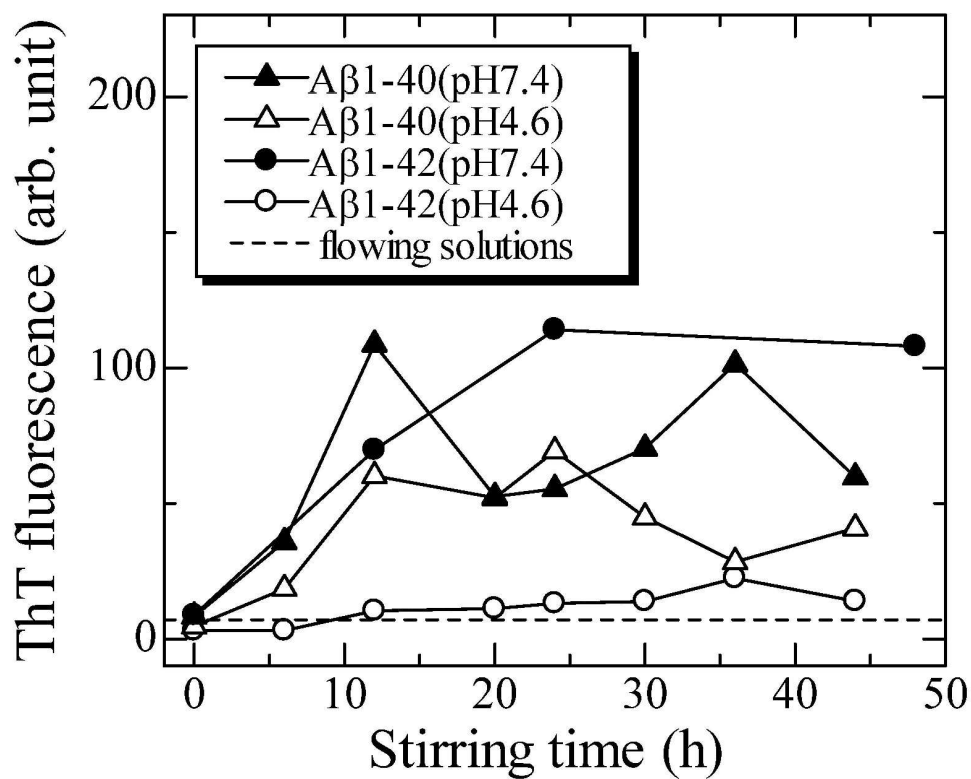
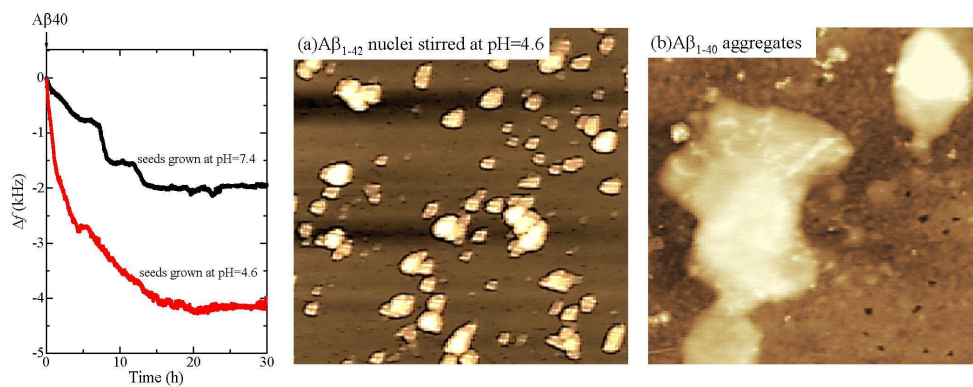


Fig. 8  
137x109mm (600 x 600 DPI)



for TOC only  
91x38mm (600 x 600 DPI)